

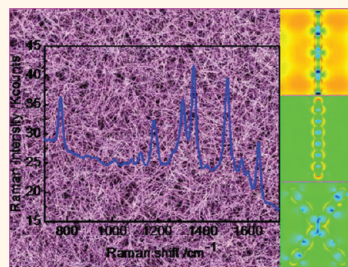
# Nanoparticle Attachment on Silver Corrugated-Wire Nanoantenna for Large Increases of Surface-Enhanced Raman Scattering

Cuifeng Tian,<sup>†</sup> Chunhua Ding,<sup>‡,\*</sup> Siyun Liu,<sup>§</sup> Shengchun Yang,<sup>†</sup> Xiaopong Song,<sup>†</sup> Bingjun Ding,<sup>†</sup> Zhiyuan Li,<sup>§,\*</sup> and Jixiang Fang<sup>†,‡,\*</sup>

<sup>†</sup>School of Science, MOE Key Laboratory for Nonequilibrium Synthesis and Modulation of Condensed Matter and <sup>‡</sup>School of Aerospace, Xi'an Jiaotong University, Shann Xi 710049, People's Republic of China, <sup>§</sup>Institute of Physics, Chinese Academy of Sciences, Beijing 100090, People's Republic of China, and <sup>‡</sup>Institut für Nanotechnologie, Karlsruhe Institut für Technologie (KIT), Karlsruhe 76021, Germany

Since the SERS effect was discovered in 1974,<sup>1</sup> it has been used widely in the detection of molecules for the possibility of enhancing the Raman emission of molecules adsorbed onto a metal surface<sup>2</sup> or metal compound surface with metal decoration.<sup>3</sup> Its sensitivity was dominated by the electromagnetic enhancement due to localized plasmon resonances, which is influenced by some general factors, such as size, shape, gap distance, wavelength, and polarization of the incident light.<sup>4,5</sup> Up to now, many efforts have been made to explore new SERS substrates with high sensitivity and reproducibility through the use of electron beam lithography,<sup>6</sup> notably nanosphere lithography,<sup>7</sup> electrospinning technique,<sup>8</sup> as well as the simple and low-cost chemosynthesis method for single-nanoparticle SERS.<sup>9–13</sup> On the other hand, the major studies of SERS have also focused on understanding how light interacts with matter at the nanometer scale using some new techniques. For example, electron energy loss spectroscopy (EELS), combined with recent developments in spectrum imaging and data processing, has been used to observe the energy and distribution of surface plasmons.<sup>14–16</sup> Tip-enhanced Raman spectroscopy (TERS)-based method has also been used to figure out the correlation between TERS signals and the morphological changes of nanostructures.<sup>17,18</sup> In addition, some researchers have started the theoretical<sup>19</sup> and experimental<sup>20</sup> work to investigate the influence of fine geometric nanostructures on local field enhancement, which is capable of improving the enhancement factor and better understanding of subtle physical mechanism of SERS.

**ABSTRACT** Using three-dimensional finite-difference time-domain (FDTD) simulation, we described a systematic investigation on the electric field enhancement of the silver corrugated nanowires. The enhancement factor (EF) of surface-enhanced Raman scattering (SERS) for corrugated nanowires can be markedly increased by 1 or 2 orders of magnitude as compared with the smooth nanowires. Moreover, the EF can be further increased with nanoparticle attachment on the corrugated Ag nanowires owing to the coupling between the discrete plasmon state of the nanoparticles and continuum plasmon states of the corrugated nanowire or the crossed corrugated nanowires. The surface plasmonic field distribution of Ag nanowires can be effectively controlled by the polarization of the incident light. Raman spectrum measurements show that the relatively dense corrugated nanowires exhibit a relatively high reproducibility and SERS enhancement attributed to the elimination of polarization-dependent SERS—anisotropic enhancement *via* the overlapping of randomly distributed Ag nanowires. Such nanostructures as potential nanoantennas offer a route to optimize plasmon coupling for designing miniaturization integration.



**KEYWORDS:** nanoantenna · corrugated nanowires · SERS · FDTD

Nanostructured substrates for SERS are expected to be anisotropic in terms of the local surface plasmon resonances (SPR),<sup>21</sup> which are created by strong electromagnetic coupling between adjacent metallic nanostructures. If probe molecules are located in such nanogaps as local Raman “hot spots”, the Raman scattering can be enhanced strongly due to local electromagnetic field enhancements. Many researchers have reported a SERS signal with respect to polarization on the coupled metallic nanowires.<sup>22,23</sup> While others showed the polarization-dependent coupling between

\* Address correspondence to chding@mail.xjtu.edu.cn, lizy@aphy.iphy.ac.cn, jxfang@mail.xjtu.edu.cn.

Received for review May 31, 2011 and accepted November 7, 2011.

Published online November 07, 2011  
10.1021/nn203889d

© 2011 American Chemical Society

the collective surface plasmon modes of two identical particles.<sup>24–26</sup> Xu's group has studied the polarization dependence of SERS in the coupled gold nanoparticle–nanowire system for nanoparticles with a variety of shapes.<sup>19</sup> Recent investigations have further extended into the plasmon propagation along thin metallic nanowires as highly promising plasmonic waveguides in photonic and electronic devices.<sup>27,28</sup> A side-by-side arrangement of a nanocross and a nanobar geometry was introduced as a new building block for coherently coupled localized surface plasmon resonance (LSPR) nanocavities.<sup>29</sup> However, although the plasmon coupling phenomenon for nanowires system has been extensively reported from both theories and experiments, even in crossed nanowires, the influence of the coupling in corrugated nanowire networks with the attachment of nanoparticles on the SERS enhancement has not yet been investigated in detail.

In this article, we have studied the size, shape, and polarization dependence of local field distributions in five models of Ag nanostructures through three-dimensional finite-difference time-domain (FDTD) simulation. By the calculation of the electromagnetic field enhancement of different models of nanowires, we were able to evaluate how the fine geometrical configurations of metal nanostructures, for example, corrugated nanowires, or nanoparticle-attached corrugated nanowires, influence the enhancement factor (EF) of SERS relative to smooth nanowires. Both the experimental and simulation results show that relatively dense overlapped nanowire networks exhibit a high reproducibility and SERS enhancement owing to the formation of homogeneously distributed hot spots and the interwire effect.

## RESULTS AND DISCUSSION

Ag corrugated nanowires were synthesized within a 3D electrochemical deposition system by using two silver electrodes and an unusually high overpotential within the deionized water. Figure 1a shows the scanning electron microscopy (SEM) image of Ag nanowires obtained via the electrodeposition for 30 min in 40 mL deionized water, which reveals that the products consist of a large area of dense nanowire networks (see also Figure S1a,b in the Supporting Information). The SEM image of relatively loose nanowires is presented in Figure S1c. From the magnified image of Figure 1a, the Ag nanowires demonstrate the irregular corrugation-like features with some nanoparticle attachment (Figure 1b,c). The morphology is similar to the Ag nanowires synthesized in our previous report.<sup>30</sup> The interval between two nodes varies from ~50 to ~200 nm. The widths of Ag nanowires are approximately 100–150 nm. A typical TEM image of the silver corrugated nanowires (Figure 2a) and its corresponding selected area electron diffraction (SAED) pattern (Figure 2b) further reveal that each segment is a single

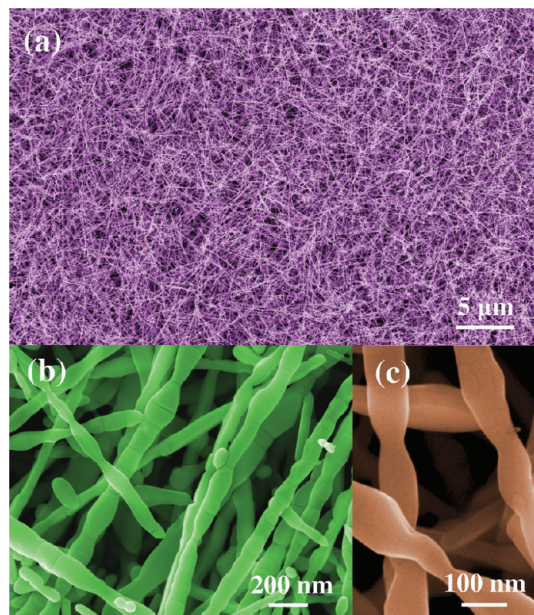


**Figure 1.** (a) SEM image of the silver nanoparticle-attached corrugated nanowires synthesized in pure water under 30 V applied potential and 30 min electrodeposition time. (b,c) High-magnification images of corrugated Ag nanowires.

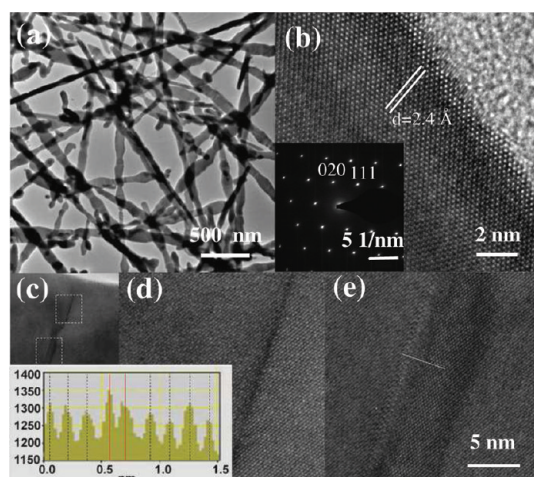


**Figure 2.** (a,b) TEM image and HRTEM image of an individual Ag corrugated nanowire (its SAED pattern shown in the inset). (c) Magnified image of one knot of corrugated nanowire, (d,e) HRTEM images of knot indicated with dashed squares in the image of panel c. The inset in panel c shows the crystallographic defect along the white line in panel e.

crystal and growing along  $\langle 111 \rangle$  directions. The joint of nodes was investigated in more detail from the HRTEM image (Figure 2c), which shows that crystallographic defects existed in the corrugation-like Ag nanowire (Figure 2d,e).

Owing to their unique geometrical configurations, we utilized these corrugated nanowires as SERS substrates by using crystal violet (CV) as the detection molecule. The Raman image of the relatively sparse Ag corrugated nanowires is shown in Figure 3a, obtained

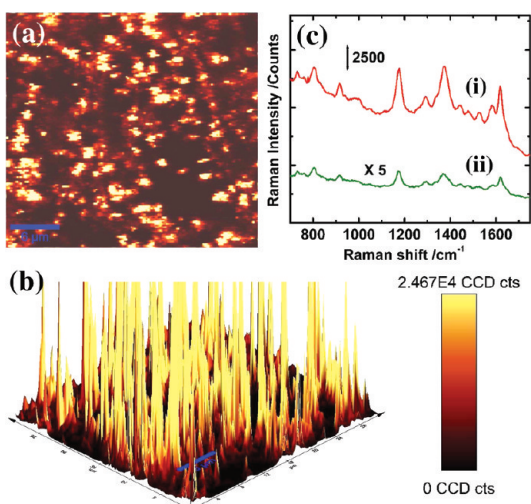


**Figure 3.** (a) Two- and (b) three-dimensional Raman images of the relatively sparse Ag corrugated nanowires, displaying a color-coded area by mapping the CV Raman peak at  $\sim 1172 \text{ cm}^{-1}$ . The right bar of the 3D image is the average CCD counts after subtracting background contributions. (c) SERS spectra of crystal violet adsorbed on the relatively sparse Ag corrugated nanowires at concentrations of (i)  $10^{-9} \text{ M}$  and (ii)  $10^{-10} \text{ M}$ , obtained with 633 nm excitation.

from the integration of a strong Raman band of CV molecules at  $1172 \text{ cm}^{-1}$  over  $1120\text{--}1250 \text{ cm}^{-1}$ . The 3D projections of these images are shown in Figure 3b. It is clearly seen that the hot spots over the sample are non-uniform and have polarization characteristics which will be elucidated in Figure 4. The typical SERS spectra obtained from the relatively sparse nanowires at 633 nm excitation are displayed in Figure 3c, applying a low-magnification objective ( $\sim 3 \mu\text{m}$  laser spot), 0.1 mW excitation power, and 20 s acquisition time. The SERS spectra represent the characteristic peaks of the CV molecule at 1172, 1371, and  $1619 \text{ cm}^{-1}$  and correspond well to the ordinary Raman spectra of CV molecules in the solid state and in aqueous solution. Raman peak height at  $\sim 1172 \text{ cm}^{-1}$  is about 4545 counts at the concentration of  $10^{-9} \text{ M}$  and 1590 counts at  $10^{-10} \text{ M}$ . According to the calculations of EFs for CV molecules (described in refs 10, 12, 13, and 31–34), we estimated EFs of about  $1.58 \times 10^8$  and  $5.5 \times 10^8$  for the SERS substrate assembled by relatively sparse nanowires at the above two concentrations, respectively. According to the calculations by Garcia-Vidal and Pendry<sup>35</sup> and experiential observation,<sup>23</sup> incident radiation excites a plasmon trapped in the nanogaps between cylinders, which can lead to SERS enhancements as large as  $10^7$ . It is deduced that the EF of Ag corrugated nanowires can be increased at least 1 order of magnitude as compared with smooth nanowires.

To further reveal the physical mechanism of the observed enhancements of the light emission for various Ag nanostructures, we carried out FDTD simulations of local field distributions as shown in Figure 4. Three types of simplified Ag nanostructural models

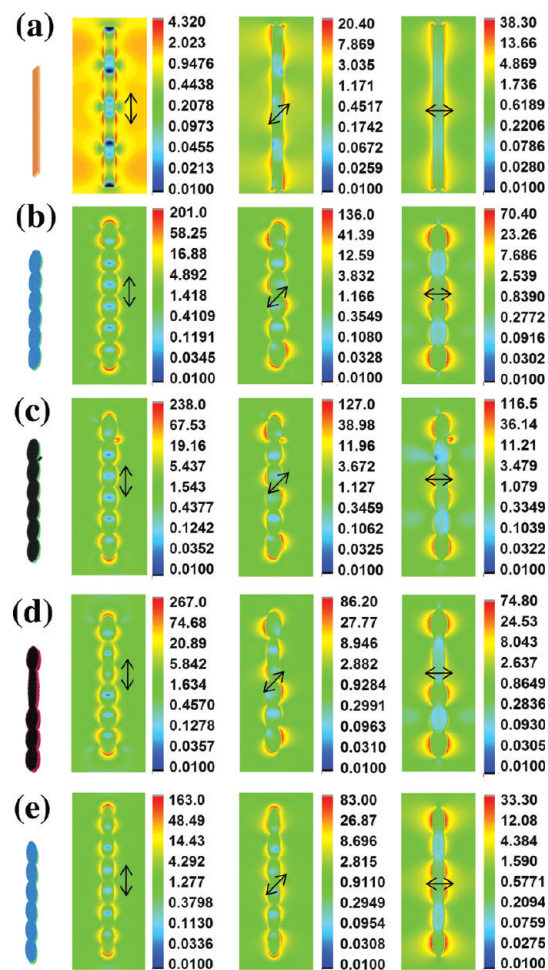


**Figure 4.** E-field amplitude patterns from theoretical calculations at the excitation wavelength of 640 nm for (a) smooth surface silver nanowire (length = 1800, width = 100, height = 50 nm). (b) Corrugated nanowire with six nodes (each node: the dimension of long axis ( $D_1$ ) is 300 nm, the dimension of short axis ( $D_2$ ) is 150 nm, joint width ( $D_3$ ) is 50 nm, the thickness ( $H$ ) is 50 nm). (c) Corrugated nanowire with one ellipsoidal particle attachment (nanowire dimension is the same as panel b, and the particle: short axis 50 nm and long axis 70 nm). (d) Irregular corrugated nanowire (second node:  $D_2 = 100 \text{ nm}$ , and other nodes are the same as the ones of panel b) and (e) narrow corrugated nanowire (each node:  $D_2 = 100 \text{ nm}$ , and other nodes are the same as the ones of panel b) and perpendicular to the incident wavevector  $k$ . The arrows represent the different polarization directions: (i)  $0^\circ$ , (ii)  $45^\circ$ , and (iii)  $90^\circ$ .

(shown in the left column of Figures 4 and Figures S2 and S3) including the smooth nanowire, corrugated nanowires and nanoparticle-attached corrugated nanowires were calculated, respectively. The geometrical parameters, optical parameters, and calculation of the enhancement factor are demonstrated in the Supporting Information. The maximal electric field strength  $|E|^2$  is found to be about 4.3, 201, and 238 for three models (the color bars of Figure 4a–c), respectively, when the polarization of the incident light is parallel to the long axis of the nanowire. For SERS, it is generally agreed that the Raman intensity increases by a factor  $|E|^4$ .<sup>20</sup> According to the FDTD calculations of

the maximum field enhancement ( $|E|^2$ ), the EF of three models can be found to increase in a series: smooth nanowire < corrugated nanowire < nanoparticle attached corrugation-like nanowire. Moreover, the EF of corrugated nanowire model (Figure 4b) can be increased by 2–3 orders of magnitude as compared with the smooth nanowire (Figure 4a). Considering that the experimental structures are more complicated and irregular than the models used in the simulations (*i.e.*, Figure 4b,c), an irregular model with a prolonged node and a reduced dimension (*i.e.*,  $D_2$ , from 150 nm for Figure 4b to 100 nm for Figure 4d) was made as shown in Figure 4d. One can clearly see that irregular corrugated nanowire demonstrates an increased field enhancement, that is, 267 for the light polarized parallel to the long axis of nanowire. In order to evaluate if the reduced dimension contributes to the increased enhancement, one more model of the corrugated nanowire with the uniform narrow node (*i.e.*,  $D_2 = 100$  nm) was also calculated (Figure 4e). Interestingly, the narrow corrugated model displays a relatively low SERS enhancement relative to the case in Figure 4b. In this regard, the introduction of the irregular node does not reduce the field enhancement. On the contrary, the irregular corrugated nanowire seems more preferable to contribute to a higher field enhancement thus an increased SERS enhancement factor.

When the polarization direction is perpendicular to the long axis (the third column), the  $|E|^2$  values are about 38.3, 70.4, and 116.5 for above three models (Figure 4a–c), respectively. This value can be increased to 20.4, 136, and 127, respectively, when the polarization direction is 45°. It is obvious that the nanostructure with curvature and dissymmetry is prone to increase the local field values. Meanwhile, all kinds of nanowires as nanoantennas can affect the local plasmon field distributions,<sup>36</sup> which are demonstrated in Figure 4. Furthermore, the incident light with various polarization directions can excite plasmons of different modes.<sup>37</sup> For the polarization parallel to the long axis of nanowires (*e.g.*, first column in Figure 4), the near field distribution is symmetrical along the direction of the long axis. When the polarization angle is increased, the symmetric nodes of the field distribution can transit from one side of the nanowire to the other. Thus, the surface plasmonic field distribution of Ag nanowires can be distinctly controlled by polarization of the incident light. At the same time, the EF of corrugated nanowire with nanoparticle attachment can be enhanced by 2–3 orders of magnitude as compared with the smooth nanowire. It is worth noting that, unlike the corrugated nanowire or other models, the smooth surface silver nanowire demonstrates a higher field enhancement for the excitation of the wire with light polarized perpendicular than parallel polarization relative to the long axis. However,

the ratio of length to width for the smooth nanowires is decreased to 1.5 (as shown in Figure S4c), the electric field for the excitation light perpendicular to the long axis is lower than that for parallel direction. Therefore, this is probably related to the aspect-ratio-dependent polarization effect of the Ag nanowires, as shown in Figure S4.

To approach the actual situation, when two or more corrugated nanowires are jointed together forming overlapped nanowire networks, we calculated the surface plasmonic field distribution of nanowires. Two kinds of crossed nanowires are shown in the left column of Figure 5, including smooth nanowires and nanoparticle-attached corrugated nanowire systems. The maximal electric field strength  $|E|^2$  is 59.6 for the smooth nanowire and 578.0 for the corrugated Ag nanowire with three nodes and nanoparticle attachment system when the polarization direction is along  $y$  axis (shown in corresponding (i) of Figure 5a,b, respectively). From the electromagnetic field distribution of the above two systems, one can find that the asymmetrical crossed and overlapped nanowire system is favorable to form a homogeneous local plasmon field by the coupling of different corrugated nanowires and nanoparticles. Although the theoretical calculations of short wire model may not capture the main characteristic of the extended corrugation-like structure, from the comparison between the models of three nodes (Figure S5) and the longer ones, we may still distill the influence of attached nanoparticle quantities and wire length on the field enhancement. When the length of crossed nanowires increases, for example, two times of model (i) in Figure 5, the field enhancement of asymmetrical corrugated nanowires is increased to 768, about 15 times higher than that of smooth nanowires (57.2 in model (ii) of Figure 5). These simulation results indicate that local fields of the corrugated Ag nanowires with nanoparticle hybrids are significantly enhanced. According to the FDTD calculations of the maximum field enhancement ( $|E|^2$ ), the crossed assembly of nanoparticle-attached corrugation-like nanowires shows an EF of ~100 times higher than that for crossed smooth nanowires. This may be attributed to the interwire effect and can be confirmed by analyzing the SERS spectra on the relatively dense silver corrugated nanowire substrate.

In above FDTD calculations, as shown in Figure 5, a contact mode between two corrugated nanowires was used. However, in the actual case of experiments, a great number of nanogaps can always be formed among the crossed silver corrugated nanowires. Therefore, some noncontact FDTD models with various nanogaps and diverse polarization directions were calculated, as are shown in Figure 6. With a small nanogap between two corrugated nanowires (*e.g.*, 1 nm), the maximal electric field strength  $|E|^2$  of 850 and 1200 can be obtained for different polarization directions, as

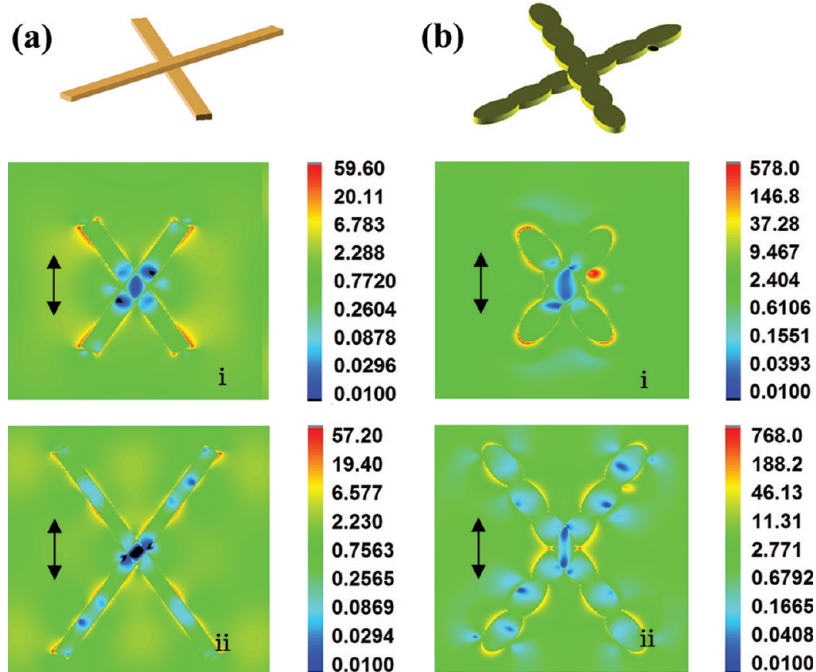


**Figure 5.** E-field amplitude patterns from theoretical calculations at the excitation wavelength of 640 nm in a plane through the intersection of the interface of (a) smooth nanowires (i)  $L = 900$  nm, (ii)  $L = 1800$  nm, and (b) nanoparticle-attached corrugation-like nanowires of (i) three nodes (each node:  $D_1 = 300$  nm,  $D_2 = 150$  nm,  $H = 50$  nm, respectively), (ii) six nodes with one particle (particle: short axis 50 nm and long axis 70 nm).

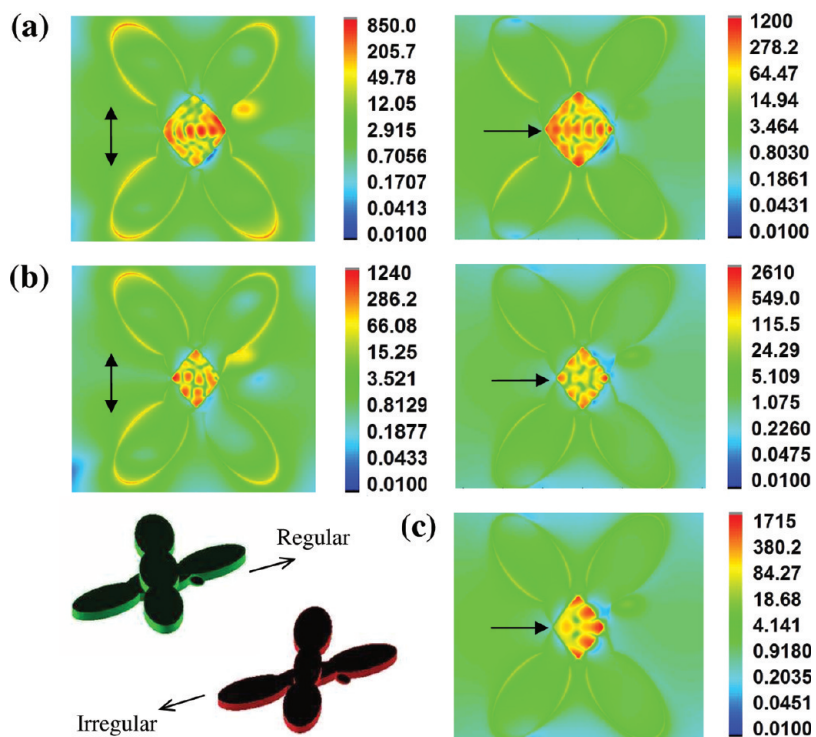


**Figure 6.** E-field amplitude patterns from theoretical calculations at the excitation wavelength of 640 nm in a plane through the intersection of the interface for (a) the nanoparticle-attached regular corrugation-like nanowires with 1 nm gap between two three-node nanowires (each node:  $D_1 = 300$  nm,  $D_2 = 150$  nm,  $H = 50$  nm, respectively); (b) nanoparticle-attached irregular corrugation-like nanowires with 1 nm gap between two three-node nanowires (second node:  $D_2 = 110$  nm, and other nodes are the same as the ones of panel a); (c) nanoparticle-attached irregular corrugation-like nanowires with 2 nm gap between two three-node nanowires. The arrows represent the polarization directions. The left bottom schematic drawings show the regular and irregular nanowires.

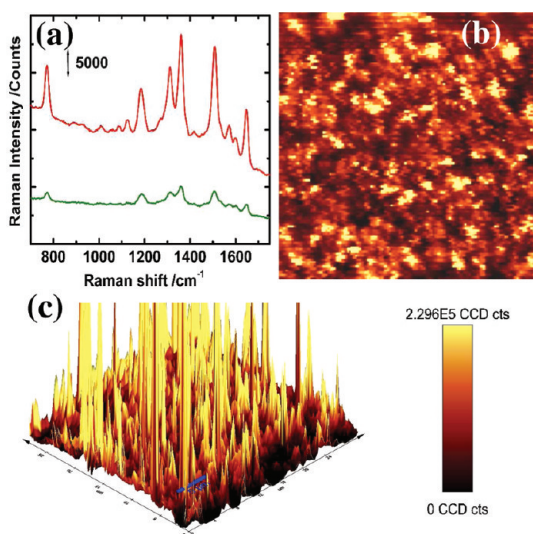


**Figure 7.** (a) SERS spectra of crystal violet adsorbed on the relatively dense Ag corrugated nanowires at CV concentrations of (i)  $10^{-9}$  M and (ii)  $10^{-10}$  M, obtained with 633 nm excitation. (b) Two- and (c) three-dimensional Raman images of the relatively dense Ag corrugated nanowires, displaying a color-coded area by mapping the CV Raman peak at  $\sim 1172 \text{ cm}^{-1}$ . The right bar of 3D image is the average CCD counts after subtracting the background contributions.

shown in Figure 6a. When an irregular nanowire model was used as shown in the bottom left of Figure 6, a further increase of field enhancement can be achieved (Figure 6b). Figure 6b demonstrates the maximal electric field strengths  $|E|^2$  for the irregular nanowire model when the nanogaps were unchanged (*i.e.*, 1 nm), which gives the values around 1200 and 2600, respectively, for different polarization directions. When the space of nanogaps was changed, for example, 2 nm (Figure 6c), the value of maximal field strength is around 1700, which is about 65% of the one with 1 nm gap (shown in the right column of Figure 6b) at the same polarization direction. According to above theoretical calculations, as the space of nanogap decrease, the pileup of electric charge and the magnitude of the charge distribution can be increased,<sup>38</sup> leading to an enhanced field coupling effect between silver nanowires. The EF of the crossed irregular corrugated nanowires with one nanoparticle in the noncontact state (right column of Figure 6b) is calculated about  $7 \times 10^6$  according to approximation of the Raman intensity by a factor  $|E|^4$ .<sup>20</sup> This value is markedly higher by 1 or 2 orders of magnitude as compared with the ones of the regular three-nodes model (see the right column of Figure 6a) and the smooth nanowire model (Figure 5a). On all accounts, based on the theoretical analysis, the EF on the Ag nanowire may be significantly enhanced when the SERS substrate consists of the multi-irregular and crossed corrugated nanowires with a certain nanogap.

The above theoretical analysis upon the crossed effect of corrugated nanowires can be experimentally demonstrated as shown in Figure 7. Figure 7a shows

typical SERS spectra of CV on the relatively dense SERS substrate assembled by nanoparticle-attached corrugation-like Ag nanowires measured with 633 nm excitation and at CV concentrations of (i)  $10^{-9}$  M and (ii)  $10^{-10}$  M, respectively. Raman peak height at  $\sim 1172 \text{ cm}^{-1}$  is about 8800 counts, which is higher than the value on the relatively sparse Ag corrugated nanowire substrate at  $10^{-9}$  M. We obtained EFs of about  $3 \times 10^8$  and  $7.1 \times 10^8$  for the relatively dense nanowires at two concentrations. Again, the EF of corrugated nanowires can be markedly enhanced by 1–2 orders of magnitude relative to the EF of smooth nanowires obtained in ref 23. In Figure 7b, a SERS image of the relatively dense Ag nanowires is displayed, and the color code represents the integrated intensity of the characteristic peak of CV at  $1172 \text{ cm}^{-1}$ . The 3D projection of the SERS image is also shown in Figure 7c. It is clearly seen that the hot spots over the dense silver corrugated nanowires are more uniform and “hotter” than those of relatively sparse corrugated nanowires (shown in Figure 3). It is proved that asymmetric structures are extremely anisotropic and have depolarization properties.<sup>39</sup>

The homogeneity and the highly bright essence of hot spots for the corrugated Ag nanowire SERS substrate shown in Figure 7 can also be deduced from the statistical results of the distribution of SERS enhancement factor and Raman “signal” density. In order to identify the difference between the sparse and dense assembled Ag nanowires, the Raman signal density was statistically recorded for only the EFs above  $10^8$ . In Figure 8a,b, we obtained the statistical distribution of the calculated EFs for the SERS substrates shown in Figure 6b and Figure 3a. Importantly, the most EF values (>95%) for the dense assembled SERS substrate are narrowly distributed in the range from  $1.0 \times 10^8$  to  $5.0 \times 10^8$ , and a small population of the EF values was observed to be above  $7 \times 10^8$ . While for the sparse assembled SERS substrate, unlike the one shown in Figure 8a, the EFs present a relatively wide distribution from  $\sim 10^7$  to  $2.0 \times 10^8$  (Figure 8b). Furthermore, the Raman signal density (EFs >  $10^8$ ) for the relatively dense corrugated nanowire SERS substrate is approximate 94% as shown in Figure 8c. This value is about 2.6 times higher than the ones for relatively sparse nanowires in the measured area. In this regard, the distribution of the SERS intensity for dense assembled corrugated Ag nanowires is more uniform than the sparse ones. According to above experimental observation, a relatively high Raman enhancement can be achieved for the dense assembled Ag nanowire SERS substrate. This is reasonable because the high density overlapping of corrugated Ag nanowires may result in abundant small nanogaps between Ag nanowires which contribute to additional bright hot spots as the description and analysis from the Figure 6. Meanwhile, the dense assembled Ag nanowire SERS substrate can also demonstrate a better signal uniformity owing to

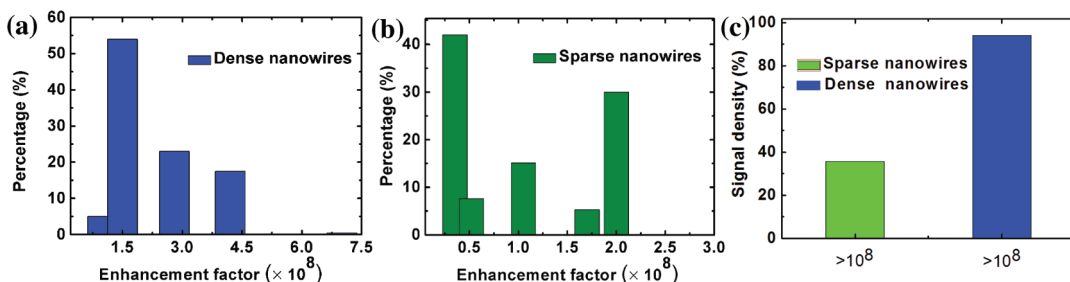


Figure 8. Distribution diagrams of the calculated enhancement factors of SERS signals for the two substrates: (a) dense assembled nanowires, (b) sparse assembled nanowires. (c) Raman “signal” density for the EFs above  $10^8$ .

the high density assembly and the depolarization effect of highly overlapped asymmetrical silver corrugated nanowires.<sup>39</sup> It is worth noting that the estimated EF value through the experimental measurement is higher than the calculated one (proportional to  $\sim |E|^4$ ) according to the FDTD simulations of the maximum field enhancement ( $|E|^2$ ). This is acceptable since chemical enhancement and surface roughness factors can be involved in actual experiments. The similar phenomena have also been observed in previous literature.<sup>10,40,41</sup>

## CONCLUSION

In summary, we have shown that the irregular and crossed corrugated Ag nanowire networks can be synthesized through a 3D electrochemical deposition. The relatively dense corrugated nanowires exhibit a relatively high reproducibility and SERS enhancement. Five simple theoretical models including smooth nanowire, corrugated nanowire, one nanoparticle attached

corrugated nanowire, irregular corrugated nanowire, and narrow corrugated nanowire have been calculated to study the relation between the high electric field enhancement and the fine structure of Ag nanowires. The surface plasmonic field distribution of nanowire can be effectively controlled by the polarization of the incident light. Moreover, the irregular corrugated nanowire seems more preferable to contribute to a higher field enhancement. Further considering the crossed mode of smooth and corrugated nanowires, it is demonstrated that the EF of overlapped corrugated nanowires can be markedly enhanced by 2–3 orders of magnitude as compared with the crossed smooth nanowires. Asymmetrical aggregated Ag corrugated nanowires are highly anisotropic, leading to high reproducibility and homogeneity of the SERS signals in the crossed corrugated nanowire networks, which is expected to have practical application as an effective SERS substrate.

## EXPERIMENTAL SECTION

**Preparation of Ag Nanowires.** Only two ingredients are required in this protocol: silver electrodes and deionized water. Two parallel electrodes of silver plate (99.995%) with dimension of  $50 \times 10 \times 0.5$  mm separated by a distance of 10 mm were immersed in deionized water. The deposition process was performed under a strong direct current (DC) potential of 30 V. After finishing the deposition process, the product is transferred to a Si substrate. Then the product was washed with ethanol and deionized water and dried at ambient temperature.

**Characterization.** The morphology and surface structure of the nanowires were characterized by scanning electron microscopy (SEM, LEO 1530). The TEM observations were performed with a FEI-Titan 80-300 operated at 300 kV. The TEM samples were prepared by carefully dropping silver suspension onto a carbon-coated TEM grid. Raman measurements were performed in backscattering geometry with a WiTec CRM200 confocal Raman microscope at the excitation wavelengths of 633 nm. Raman imaging of hot spots over silver nanostructures was performed on the CRM200 microscope employing a piezo table for sample scanning with a typical  $X-Y$  step of 200 nm ( $200 \times 200 \text{ nm}^2$  scanning pixel size), a high-resolution 100× objective ( $\sim 0.5 \mu\text{m}$  laser spot), and a spectrum acquisition time of 2 s per pixel. The Raman images represent a color-coded area of the characteristic Raman band of CV at  $1172 \text{ cm}^{-1}$  integrated over  $1120\text{--}1250 \text{ cm}^{-1}$  with a subtracted broad background signal.

**Acknowledgment.** We thank Drs S. Lebedkin, Di Wang, and F. Schramm, in Karlsruhe Institut für Technologie (KIT), Institut für Nanotechnologie, Germany, for their helpful discussions. J.X. F. was supported by National Natural Science Foundation of China (No. 51171139), Tengfei Talent Project of Xi'an Jiaotong University, the New Century Excellent Talents in University (NCET), and the Fundamental Research Funds for the Central Universities (No. 08142008). X. P. Song was supported by National Natural Science Foundation of China (No. 51071116). S. C. Yang was supported by National Natural Science Foundation of China (No. 50901056). Z.Y.L. was supported by the National Natural Science Foundation of China under Grant Nos. 60736041 and 10874238.

**Supporting Information Available:** SEM images of corrugated nanowires, details of FDTD simulation, optical parameters, and the estimation of SERS enhancement factor. This material is available free of charge via the Internet at <http://pubs.acs.org>.

## REFERENCES AND NOTES

- Fleischmann, M.; Hendra, P. J.; McQuillan, A. J. Raman Spectra of Pyridine Adsorbed at a Silver Electrode. *Chem. Phys. Lett.* **1974**, *26*, 163–166.
- Qian, X. M.; Nie, S. M. Single-Molecule and Single-Nanoparticle SERS: From Fundamental Mechanisms to Biomedical Applications. *Chem. Soc. Rev.* **2008**, *37*, 912–920.
- Feng, M.; Zhang, M.; Song, J. M.; Li, X. G.; Yu, S. H. Ultra-long Silver Trimolybdate Nanowires: Synthesis, Phase

- Transformation, Stability, and Their Photocatalytic, Optical, and Electrical Properties. *ACS Nano* **2011**, *5*, 6726–6735.
- Wang, H.; Levin, C. S.; Halas, N. J. Nanosphere Arrays with Controlled Sub-10-nm Gaps as Surface-Enhanced Raman Spectroscopy Substrates. *J. Am. Chem. Soc.* **2005**, *127*, 14992–14993.
  - Tabor, C.; Murali, R.; Mahmoud, M.; El-Sayed, M. A. On the Use of Plasmonic Nanoparticle Pairs as a Plasmon Ruler: The Dependence of the Near-Field Dipole Plasmon Coupling on Nanoparticle Size and Shape. *J. Phys. Chem. A* **2009**, *113*, 1946–1953.
  - Kubo, W.; Fujikawa, S. Au Double Nanopillars with Nano-gap for Plasmonic Sensor. *Nano Lett.* **2011**, *11*, 8–15.
  - Yang, S. K.; Xu, F.; Ostendorp, S.; Wilde, G.; Zhao, H. P.; Lei, Y. Templated-Confining Dewetting Process to Surface Nano-patterns: Fabrication, Structural Tunability, and Structure-Related Properties. *Adv. Mater.* **2011**, *21*, 2446–2455.
  - He, D.; Hu, B.; Yao, Q. F.; Wang, K.; Yu, S. H. Large-Scale Synthesis of Flexible Free-Standing SERS Substrates with High Sensitivity: Electrospun PVA Nanofibers Embedded with Controlled Alignment of Silver Nanoparticles. *ACS Nano* **2009**, *3*, 3993–4002.
  - Wang, H.; Halas, N. J. Mesoscopic Au “Meatball” Particles. *Adv. Mater.* **2008**, *20*, 820–825.
  - Fang, J. X.; Du, S. Y.; Lebedkin, S.; Li, Z. Y.; Krulk, R.; Kappes, M.; Hahn, H. Gold Mesostructures with Tailored Surface Topography and Their Self-Assembly Arrays for Surface-Enhanced Raman Spectroscopy. *Nano Lett.* **2010**, *10*, 5006–5013.
  - Liang, H. Y.; Li, Z. P.; Wang, W. Z.; Wu, Y. S.; Xu, H. X. Highly Surface-Roughened “Flower-Like” Silver Nanoparticles for Extremely Sensitive Substrates of Surface-Enhanced Raman Scattering. *Adv. Mater.* **2009**, *21*, 4614–4618.
  - Fang, J. X.; Liu, S. Y.; Li, Z. Y. Polyhedral Silver Mesocages for Single Particle Surface-Enhanced Raman Scattering-Based Biosensor. *Biomaterials* **2011**, *32*, 4877–4884.
  - Fang, J. X.; Lebedkin, S.; Yang, S. C.; Hahn, H. A New Route for the Synthesis of Polyhedral Gold Mesocages and Shape Effect in Single-Particle Surface-Enhanced Raman Spectroscopy. *Chem. Commun.* **2011**, *47*, 5157–5159.
  - Nelayah, J.; Kociak, M.; Stephan, O.; Abajo, F. J. G.; Tence, M.; Henrard, L.; Taverna, D.; Pastoriza-Santos, I.; Liz-Marzan, L. M.; Colliex, C. Mapping Surface Plasmons on a Single Metallic Nanoparticle. *Nat. Phys.* **2007**, *3*, 348–353.
  - Song, F. Q.; Wang, T. Y.; Wang, X. F.; Xu, C. H.; He, L. B.; Wan, J. G.; Haesendonck, C. V.; Ringer, S. P.; Han, M.; Liu, Z. W.; et al. Visualizing Plasmon Coupling in Closely Spaced Chains of Ag Nanoparticles by Electron Energy-Loss Spectroscopy. *Small* **2010**, *6*, 446–451.
  - N’Gom, M.; Ringnalda, J.; Mansfield, J. F.; Agarwal, A.; Kotov, N.; Zaluzec, N. J.; Norris, T. B. Single Particle Plasmon Spectroscopy of Silver Nanowires and Gold Nanorods. *Nano Lett.* **2008**, *8*, 3200–3204.
  - Zhang, W. H.; Schmid, T.; Yeo, B. S.; Zenobi, R. Near-Field Heating, Annealing, and Signal Loss in Tip-Enhanced Raman Spectroscopy. *J. Phys. Chem. C* **2008**, *112*, 2104–2108.
  - Zhang, W. H.; Cui, X. D.; Yeo, B. S.; Schmid, T.; Hafner, C.; Zenobi, R. Nanoscale Roughness on Metal Surfaces Can Increase Tip-Enhanced Raman Scattering by an Order of Magnitude. *Nano Lett.* **2007**, *7*, 1401–1405.
  - Wei, H.; Hao, F.; Huang, Y. Z.; Wang, W. Z.; Nordlander, P.; Xu, H. X. Polarization Dependence of Surface-Enhanced Raman Scattering in Gold Nanoparticle–Nanowire Systems. *Nano Lett.* **2008**, *8*, 2497–2502.
  - Dawson, P.; Duenas, J. A.; Boyle, M. G.; Doherty, M. D.; Bell, S. E. J. Combined Antenna and Localized Plasmon Resonance in Raman Scattering from Random Arrays of Silver-Coated, Vertically Aligned Multiwalled Carbon Nanotubes. *Nano Lett.* **2011**, *11*, 365–371.
  - Kreibig, U.; Vollmer, M. *Optical Properties of Metal Clusters*; Springer: New York, 1995.
  - Jeong, D. H.; Zhang, Y. X.; Moskovits, M. Polarized Surface Enhanced Raman Scattering from Aligned Silver Nanowire Rafts. *J. Phys. Chem. B* **2004**, *108*, 12724–12728.
  - Tao, A. R.; Yang, P. D. Polarized Surface-Enhanced Raman Spectroscopy on Coupled Metallic Nanowires. *J. Phys. Chem. B* **2005**, *109*, 15687–15690.
  - Xu, H. X.; Käll, M. A New Method by Extending Mie Theory To Calculate Local Field in Outside/Inside of Aggregates of Arbitrary Spheres. *ChemPhysChem* **2003**, *4*, 1001–1005.
  - Etchegoin, P. G.; Galloway, C.; Le Ru, E. C. Polarization-Dependent Effects in Surface-Enhanced Raman Scattering (SERS). *Phys. Chem. Chem. Phys.* **2006**, *8*, 2624–2628.
  - Camargo, P. H. C.; Rycenga, M.; Au, L.; Xia, Y. N. Isolating and Probing the Hot Spot Formed between Two Silver Nanocubes. *Angew. Chem., Int. Ed.* **2009**, *48*, 2180–2184.
  - Li, Z. P.; Hao, F.; Huang, Y. Z.; Fang, Y. R.; Nordlander, P.; Xu, H. X. Directional Light Emission from Propagating Surface Plasmons of Silver Nanowires. *Nano Lett.* **2009**, *9*, 4383–4386.
  - Wei, H.; Ratchford, D.; Li, X. Q.; Xu, H. X.; Shih, C. K. Propagating Surface Plasmon Induced Photon Emission from Quantum Dots. *Nano Lett.* **2009**, *9*, 4168–4171.
  - Verellen, N.; Dorpe, P. V.; Huang, C. J.; Lodewijks, K.; Vandebosch, G. A. E.; Lagae, L.; Moshchalkov, V. V. Plasmon Line Shaping Using Nanocrosses for High Sensitivity Localized Surface Plasmon Resonance Sensing. *Nano Lett.* **2011**, *11*, 391–397.
  - Fang, J. X.; Hahn, H.; Krupe, R.; Schramm, F.; Scherer, T.; Ding, B. J.; Song, X. P. Silver Nanowires Growth via Branch Fragmentation of Electrochemically Grown Silver Dendrites. *Chem. Commun.* **2009**, 1130–1132.
  - Wang, Y.; Becker, M.; Wang, L.; Liu, J. Q.; Scholz, R.; Peng, J.; Gösele, U.; Christainse, S. H.; Kim, D. H.; Steinhart, M. Nanostructured Gold Films for SERS by Block Copolymer-Templated Galvanic Displacement Reactions. *Nano Lett.* **2009**, *9*, 2384–2389.
  - Cai, W. B.; Ren, B.; Li, X. Q.; She, C. X.; Liu, F. M.; Cai, X. W.; Tian, Z. Q. Investigation of Surface-Enhanced Raman Scattering from Platinum Electrodes Using a Confocal Raman Microscope: Dependence of Surface Roughening Pretreatment. *Surf. Sci.* **1998**, *406*, 9–22.
  - Le Ru, E. C.; Blackie, E.; Meyer, M.; Etchegoin, P. G. Surface Enhanced Raman Scattering Enhancement Factors: A Comprehension Study. *J. Phys. Chem. C* **2007**, *111*, 13794–13803.
  - Ren, B.; Liu, G. K.; Lian, X. B.; Yang, Z. L.; Tian, Z. Q. Raman Spectroscopy on Transition Metals. *Anal. Bioanal. Chem.* **2007**, *388*, 29–45.
  - Garcia-Vidal, F. J.; Pendry, J. B. Collective Theory for Surface Enhanced Raman Scattering. *Phys. Rev. Lett.* **1996**, *77*, 1163–1166.
  - Giannini, V.; Fernández-Domínguez, A. I.; Heck, S. C.; Maier, S. A. Plasmonic Nanoantennas: Fundamentals and Their Use in Controlling the Radiative Properties of Nanoemitters. *Chem. Rev.* **2011**, *111*, 3888–3912.
  - Fang, Y. R.; Li, Z. P.; Huang, Y. Z.; Zhang, S. P.; Nordlander, P.; Halas, N. J.; Xu, H. X. Branched Silver Nanowires as Controllable Plasmon Routers. *Nano Lett.* **2010**, *10*, 1950–1954.
  - Romero, I.; Aizpurua, J.; Bryant, G. W.; Garcia de Abajo, F. J. Plasmons in Nearly Touching Metallic Nanoparticles: Singular Response in the Limit of Touching Dimers. *Opt. Express* **2006**, *14*, 9988–9999.
  - Bosnick, K. A.; Jiang, J.; Brus, L. E. Fluctuations and Local Symmetry in Single-Molecule Rhodamine 6G Raman Scattering on Silver Nanocrystal Aggregates. *J. Phys. Chem. B* **2002**, *106*, 8096–8099.
  - Wustholz, K. L.; Henry, A. I.; McMahon, J. M.; Freeman, R. G.; Valley, N.; Piotti, M. E.; Natan, M. J.; Schatz, G. C.; Duyne, R. P. V. Structure–Activity Relationships in Gold Nanoparticle Dimers and Trimers for Surface-Enhanced Raman Spectroscopy. *J. Am. Chem. Soc.* **2010**, *132*, 10903–10910.
  - Lim, D. K.; Jeon, K. S.; Hwang, J. H.; Kim, H.; Kwon, S.; Suh, Y. D.; Nam, J. M. Highly Uniform and Reproducible Surface-Enhanced Raman Scattering from DNA-Tailorable Nanoparticles with 1-nm Interior Gap. *Nat. Nanotechnol.* **2011**, *6*, 452–460.